

MATERobot: Material Recognition in Wearable Robotics for People with Visual Impairments

Junwei Zheng^{1,*}, Jiaming Zhang^{1,*}, Kailun Yang^{2,†}, Kunyu Peng¹, and Rainer Stiefelhagen¹

Abstract— Wearable robotics can improve the lives of People with Visual Impairments (PVI) by providing additional sensory information. Blind people typically recognize objects through haptic perception. However, *knowing materials before touching* is under-explored in the field of assistive technology. To fill this gap, in this work, a wearable robotic system, MATERobot, is established for PVI to recognize materials before hand. Specially, the human-centric system can perform pixel-wise semantic segmentation of objects and materials. Considering both general object segmentation and material segmentation, an efficient *MateViT* architecture with *Learnable Importance Sampling (LIS)* and *Multi-gate Mixture-of-Experts (MMoE)* is proposed to wearable robots to achieve complementary gains from different target domains. Our methods achieve respective 40.2% and 51.1% of mIoU on COCOStuff and DMS datasets, surpassing previous method with +5.7% and +7.0% gains. Moreover, on the field test with participants, our wearable system obtains a score of 28 in NASA-Task Load Index, indicating low cognitive demands and ease of use. Our MATERobot demonstrates the feasibility of recognizing material properties through visual cues, and offers a promising step towards improving the functionality of wearable robots for PVI. Code will be available at: <https://github.com/JunweiZheng93/MATERobot>.

I. INTRODUCTION

Material recognition is a crucial task in the application of scene understanding and has a wide range of usage scenarios. The prediction of material recognition can provide additional *material* information (1) to support robotic grippers [1] to determine the correct force when grasping or holding fragile *glass* objects, (2) to assist autonomous vehicles to switch to the appropriate driving mode on *sandy* roads with a low resistance coefficient [2], (3) to warn people if they put *plastic* objects in the microwave, and (4) to alert People with Visual Impairments (PVI) to slippery surfaces [3], [4] when walking on *snowy* sidewalks. To this end, the task of material recognition is of critical importance in real-world scenarios.

In addition to the above specific cases, material recognition in everyday life is often a challenging task for PVI, who typically recognize object through touch [5], [6]. Therefore, it becomes vital to develop a system that can assist PVI in recognizing the materials of objects before touch, *i.e.*, a

This work was supported in part through the AccessibleMaps project by the Federal Ministry of Labor and Social Affairs (BMAS) under the Grant No. 01KM15112, in part by the “KIT Future Fields” project, in part by the Helmholtz Association Initiative and Networking Fund on the HAICORE@KIT partition, and in part by Hangzhou SurImage Technology Company Ltd. ([†]Correspondence: Kailun Yang.)

*Equal contribution.

¹Institute for Anthropomatics and Robotics, Karlsruhe Institute of Technology, Germany. Email: junweizheng.cn@outlook.com, first-name.lastname@kit.edu.

²School of Robotics, Hunan University, China. Email: kailun.yang@hnu.edu.cn.

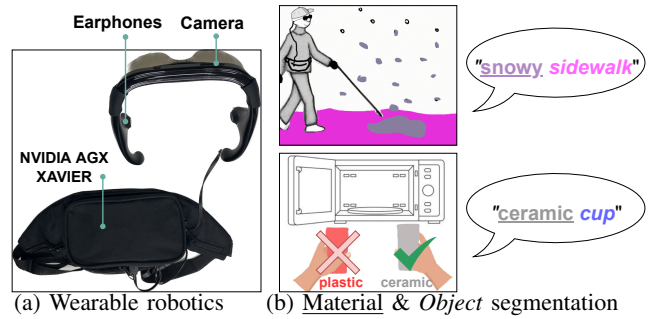


Fig. 1: MATERobot, (a) wearable robotics, can assist (b) material semantic segmentation (*e.g.*, *snow*, *ceramic*) and general object semantic segmentation (*e.g.*, *sidewalk*, *cup*)

contact-free material recognition system. Thus, in this work, we mainly focus on designing a human-friendly wearable device for PVI to recognize materials. In recent years, significant progress has been witnessed in the field of assistive technology that can support PVI in several activities, such as navigation [7], object localization [8], indoor understanding [9], and path orientation [10]. While panoptic predictions were provided in [4], transparent objects were recognized in [10], both can only deliver limited material categories.

In this paper, general and material recognition in wearable robotic systems are presented, *i.e.*, **MATERobot**. As shown in Fig. 1a, such a human-friendly system consists of a pair of smart glasses with a RGB-D camera and a pair of bone-conducting earphones, and a portable image processor inside a small waist bag. In Fig. 1b, the MATERobot can recognize not only materials (*e.g.*, *snow*), but also general object categories (*e.g.*, *sidewalk*). These two predictions from different fields can form a feedback of object categories with material properties (*e.g.*, “*snowy sidewalk*”), yielding more comprehensive information to assist PVI in their daily life.

Due to the bottleneck of self-attention in dense prediction [11], it is, however, hard to deploy a resource-intensive ViT-based model on wearable robotic platforms. To address this challenge, compared to the ViT-based counterparts [11], we propose an efficient material segmentation ViT-based model, namely **MateViT**, which includes a **Learnable Importance Sampling (LIS)** strategy to maintain only the informative tokens for the material segmentation, so as to reduce the computational cost. Based on our LIS method, a resource-friendly MateViT model is obtained, which makes it feasible to deploy plain vision transformers on wearable robotic devices that have limited computational resources.

Apart from the model efficiency, to enlarge the model capacity, we introduce a **Multi-gate Mixture-of-Experts (MMoE)** method to combine the aforementioned general image semantic segmentation and material semantic segmentation on a single model. Compared to the previous method [10] using a straightforward dual-head structure, our MMoE is proposed to construct an efficient multi-task learning architecture. The feature tokens from input images are forwarded to respective gates and experts to extract the top- k informative features for task-relevant decoder heads that generate final semantic segmentation masks.

In order to endow MATERobot with robust perception capability, including general and material semantic segmentation, we perform model training on COCOSTuff-10K [12] and DMS [13] datasets, both contain more than 10K training samples. Through extensive experiments, our small model obtains 40.2% and 51.1% of mIoU scores, surpassing the previous multi-task learning baseline [10] by absolute +5.7% and +7.0% on COCOSTuff-10K and DMS, respectively. For single-task learning on materials segmentation, *i.e.*, on DMS, our model reaches state-of-the-art performance, having +8.1% mIoU gains compared to previous CNN counterpart [13]. To verify the practicability of our MATERobot for recognizing material categories in real-world scenarios, we conduct a task-oriented user study with six blindfolded participants. On the post-study questionnaires, our system obtains respective 28 and 77 scores regarding the evaluation criteria of NASA-Task Load Index (NASA-TLX) and System Usability Scale (SUS), which indicates the ease of use and the usability of our MATERobot in practical scenarios.

In summary, our main contributions are:

- We consider material recognition in assistive technology for the first time, and build a wearable robotic system, *i.e.*, MATERobot, for people with visual impairments to realize contactless material recognition in daily life.
- We propose an efficient *MateViT* model to enable the deployment of resource-intensive ViT-based counterparts on resource-constrained mobile platforms by using a *Learnable Importance Sampling (LIS)* strategy.
- We present a *Multi-gate Mixture-of-Experts (MMoE)* method for efficient multi-task learning and the combination of general and material semantic segmentation.
- We conduct a task-oriented user study and a post-study questionnaire session with six blindfolded participants. Through quantitative and qualitative analyses, the usability and effectiveness of our MATERobot are proved.

II. RELATED WORK

A. Wearable Assistive System

With the tremendous capability revealed by computer vision algorithms, vision-based wearable assistance systems [3], [14], [15] are becoming increasingly applicable. A vision-based navigation system [7], calculating precise positions and orientations, is proposed to help People with Visual Impairments (PVI) stay on track during walking, and it can recognize unexpected dynamic obstacles, to reduce

the danger on navigation. Due to the COVID-19 pandemic, an object-finding algorithm is introduced in [8] to build an end-to-end perception robotic cane system, which can enable socially-preferred autonomous goal selection and navigation in indoor spaces. Specifically, an algorithm for social norm-aware chair selection is proposed, which is optimized for convenience, intimacy, and privacy, respectively. In [9], a lightweight system with a solid-state LiDAR sensor is proposed for holistic indoor detection and avoidance, by using 3D point cloud instance segmentation. In this system, obstacle avoidance and object finding are implemented together with voice guidance, so that new point cloud from a changing indoor environment can be scanned by the user. In a previous work [10], to cover segmentation of the safety-critical transparent objects, a dual-head transformer model is proposed and deployed on a wearable device for helping PVI to recognize the glass-like objects in everyday life. However, only limited recognizable materials are delivered in previous wearable assistance systems. In order to help blind users to obtain a more comprehensive and humanized experience on material recognition, we design a wearable robotic system in this work, for the first time, which can not only recognize conventional object categories, such as *cups*, but also further recognize the material of the object, such as *plastic cups*, delivering contactless object recognition.

B. Material Semantic Segmentation

In Fully Convolutional Networks (FCNs) [16], image semantic segmentation is addressed as a dense-pixel classification task in an end-to-end manner. In order to achieve better performance, previous works [17], [18] focus on extracting contextual information or using multi-scale features [19]. However, the limited receptive field captured by FCNs is hard to model the correlations among long-range spatial locations. Recently, Vision Transformer [11], [20] is proposed to utilize the self-attention operation in transformer layers to extract non-local features from a sequence of image patches, yielding an alternative backbone solution compared to convolutional counterparts [19], [18], [21]. In DMS [13], a model based on ResNet [21] is used to address dense material segmentation. In contrast to DMS [13], we adopt Vision Transformer as the backbone, *e.g.*, ViT [11], to perform material semantic segmentation, with the aim of extracting long-distance dependencies between image patches, since the long-range contextual information is crucial for robust representation of diverse materials [10]. However, due to the high computational demanding of self-attention operation, there is still a bottleneck when deploying a plain vision transformer on resource-constrained mobile platforms, *e.g.* mobile robots and wearable devices. In this work, we propose a novel importance sampling method to reduce the number of token and maintain only the informative ones for material segmentation, so as to enable the deployment of plain vision transformers on wearable devices.

III. MATEROBOT: A WEARABLE ROBOTIC SYSTEM

In this section, we introduce MATERobot, *i.e.*, the wearable robotic system for material recognition, including the hardware components in Sec. III-A, the user interaction in Sec. III-B, the overall model architecture as algorithm in Sec. III-C, our efficient ViT with Learnable Importance Sampling (LIS) in Sec. III-D, and the Multi-gate Mixture-of-Experts (MMoE) in Sec. III-E.

A. Hardware Component

As shown in Fig. 1a, there are three main hardware components in our MATERobot, including a pair of KRVision smart vision glasses¹, a portable processor, and a power bank inside a waist bag. Inside the smart glasses, there are an RGB-Depth camera RealSense R200² and a pair of bone-conduction headphones. For the concept of human-friendly design, there are three advantages of using bone-conduction earphones, which are comfortable to wear, clean and hygienic, and keep in touch with the outside world. Maintaining awareness of ambient sounds is especially important for PVI. Besides, in order to maintain higher portability of the system, we choose the smaller NVIDIA Jetson AGX Xavier³ on the market, which brings suitable compute density, energy efficiency, and higher inference capabilities. Furthermore, a power bank with high energy capacity is selected to provide the system with up to 6 hours of battery life, which greatly reduces the battery life anxiety of traditional wearable devices [9]. Through the above hardware components, a more portable MATERobot and better user experience can be delivered to PVI when performing contactless material recognition in real-world scenarios.

B. User Interaction

Between the system and the user, we design an easy-to-use interface for PVI. First of all, in order to give users timely information feedback, we adopt an adjustable feedback frequency. For example, if users set a larger interval in a more familiar environment, *e.g.*, home, they will get concise information. If they explore an unknown space, setting a high frequency can obtain more information. Besides, between the pixel-wise image segmentation results to the auditory output to users, only the detected object and material that locate in the middle of the input image will be selected. Their pre-defined texts are used to generate speeches jointly in form of “material objects”, such as “ceramic cups” or “metal forks”.

C. MateViT Model

Apart from the hardware components, we further detail the overall model architecture deployed on MATERobot. Vision Transformer (ViT) [11] outperforms other counterparts, *e.g.*, CNNs, in many different computer vision tasks, and therefore, it is widely used as the backbone in various concurrent methods. For the sake of achieving high performance and efficiency, we propose *MateViT*, which has ViT [11]

with *Learnable Importance Sampling (LIS)* as the backbone, followed by an upsampling layer, a *Multi-gate Mixture-of-Experts (MMoE)* layer and two decoder heads. The overall architecture is shown in Fig. 2. Note that our multi-task learning architecture can be easily extended to more tasks by adding decoder heads. Mixed by two different datasets, each input data sample is first encoded by the efficient ViT backbone and then fed into the upsampling layer. One gate in the MMoE layer is corresponding to one task, receiving the data sample that is only relevant to the task. Depending on the output of the gate, different selected experts are activated to learn meaningful latent representations, which are finally decoded by the task-relevant decoder head. Different from the training process, one data sample is fed into all gates synchronously during inference, and latent representations from selected experts are then decoded by corresponding decoder heads, producing predictions for all tasks.

D. Learnable Importance Sampling

Although ViT [11] shows excellent potential in computer vision tasks, the computation cost explodes with high-resolution input images. Prior works expedite ViT [11] by reducing image token numbers, *e.g.* EViT [24]. In order to make vanilla ViT [11] more lightweight and feasible in real-world applications, we propose a Learnable Importance Sampling strategy for material semantic segmentation, yielding an efficient MateViT. Our approach does not require an additional class token in forward pass compared to EViT [24]; therefore, it further reduces the model complexity with high-resolution inputs. As illustrated in Fig. 2, all image patches are flattened and projected into tokens, forming Queries (**Q**), Keys (**K**), and Values (**V**). Multi-Head Self-Attention (MHSA) is then calculated as:

$$MHSA(\mathbf{Q}, \mathbf{K}, \mathbf{V}) = \text{Softmax}\left(\frac{\mathbf{Q}\mathbf{K}^T}{\sqrt{C}}\right)\mathbf{V} \quad (1)$$

where $\mathbf{Q} \in \mathbb{R}^{N \times C}$, $\mathbf{K} \in \mathbb{R}^{N \times C}$ and $\mathbf{V} \in \mathbb{R}^{N \times C}$ are query, key and value matrices; N , C are token number and dimension. Since softmax is introduced in attention map calculation, the summation of each value in rows is equal to 1. However, the result does not always equal 1 when summing up all values in columns, indicating the importance of each token from an image. Based on this observation, we first calculate the summation in columns and then average the importance vectors among all heads. Top k values are selected and tokens are downsampled according to the indices of these k values after *Add & Norm*, which stand for a residual link [21] and layer normalization [25]. Fig. 2 illustrates the whole LIS process in detail. Following [22], the downsampled tokens are then sent to a Feed-Forward Network (FFN) followed by another *Add & Norm*. Since the token number is reduced after the importance sampling, an upsampling layer is then applied, which is a standard transformer decoder block [22]. Thanks to LIS, a vanilla ViT-based model is expedited and better qualified for real-world mobile applications.

¹Glasses: www.krvision.cn

²Camera: www.intelrealsense.com

³Processor: www.nvidia.com

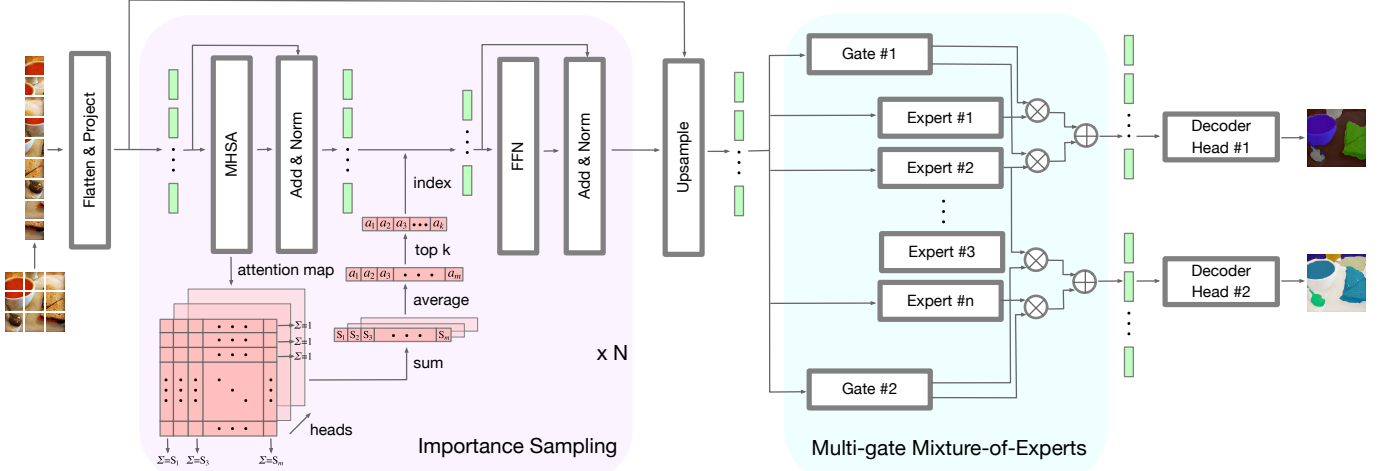


Fig. 2: **Model architecture of MateViT** in a Learnable Importance Sampling (LIS) strategy to reduce the computational complexity, and with a Multi-gate Mixture-of-Experts (MMoE) layer to perform dual-task segmentation (*i.e.*, #1-Object and #2-Material segmentation). MHSA and FFN stand for Multi-Head Self-Attention and Feed-Forward Network, respectively. The upsampling layer is a ViT-based decoder block [22]. Decoder heads are the segmentation head of Segmenter [23].

E. Multi-gate Mixture-of-Experts

Since the performance of a wearable robotic system is relevant to its model capacity, Mixture-of-Experts [26] is proposed for enlarging model capacity while maintaining invariant model complexity. However, the usage of MoE is less discussed on wearable systems [10]. For the first time, we adopt the MoE method to perform complementary training of both general object and material segmentation, *i.e.*, the former prevents the latter from overfitting and vice versa. Based on these observations, we adopt a Multi-gate Mixture-of-Experts (MMoE) layer in our model for high efficiency and performance. Fig. 2 shows the detail of the MMoE layer for multi-task learning. Specifically, one gate is responsible for one task to select the experts. Similar to [26], the resulting selection vector $G(\mathbf{x})$ can be described as:

$$G(\mathbf{x}) = \text{Softmax}(\text{TopM}(H(\mathbf{x}), m)) \quad (2)$$

$$H(\mathbf{x}) = \mathbf{x} \cdot \mathbf{W}_g + N(\mathbf{x}) \quad (3)$$

$$N(\mathbf{x}) = \text{Normal}(\text{Softplus}(\mathbf{x} \cdot \mathbf{W}_{noise})) \quad (4)$$

$$\text{TopM}(\mathbf{v}, m)_i = \begin{cases} v_i & \text{if } v_i \text{ ranks top } m \\ -\infty & \text{otherwise} \end{cases} \quad (5)$$

where \mathbf{x} , \mathbf{W}_g , and \mathbf{W}_{noise} are token, gate matrix, and noise matrix, respectively. The noise term $N(\mathbf{x})$ is calculated by the CDF of the standard normal distribution $\text{Normal}(\cdot)$ for balancing load. During the training, for every token in one image, only one same gate is activated to produce the selection vector. According to the indices of the top- m values, m experts are selected and the token is only fed into the m experts. The output of the MMoE layer is a weighted sum of the top m values in the selection vector and their corresponding outcomes from the m experts. A task-relevant decoder head [23] is then applied to transform all output tokens from MMoE into a prediction mask. Note that we also employ the load and importance balancing loss follow-

ing [26] besides the task loss. During the inference, every token from one image is fed into all gates synchronously. The resulting weighted sums from selected experts are then decoded by the corresponding decoder heads shown in Fig. 2. As the model is trained jointly on two tasks, the knowledge absorbed from object segmentation plays an important role in the high performance of material recognition, which provides PVI with accurate material information in their daily life.

IV. EXPERIMENTS

A. Settings and Datasets

Settings. We implement the model with PyTorch 1.12.1 and CUDA 11.6. The learning rate is initialized as 0.01 and it is scheduled by a cosine annealing strategy [27]. SGD with momentum 0.9 is adopted as the optimizer. We initialize our efficient ViT backbone with a pre-trained vanilla ViT [11] and keep other layers of the model randomly initialized. Data augmentations like random horizontal flipping, random resize with a ratio 0.5-2, and random cropping to 512×512 are used during training. Note that we **do not** use other tricks such as OHEM, auxiliary loss, and class-weighted loss for a fair comparison to other methods. We train our model with a batch size of 4 for 200 epochs on four 1080Ti GPUs.

Datasets. We adopt COCOSTuff-10K [12] and DMS [13] for general object and material segmentation, respectively. The COCOSTuff-10K dataset [12] has 9000/1000 images for training/testing. We conduct experiments following the implementation of mmsegmentation [28] with 171 categories. The DMS dataset [13] has respective 21857/9057/9152 images for training/validation/testing with 46 categories.

B. Results on Object Segmentation

In this experiment, we focus on a single task, *i.e.*, object segmentation on COCOSTuff-10K [12]. Referring to the model architecture, we remove the MMoE layer from the ViT-based model in order to perform the single-task learning.

TABLE I: **Results of single-task learning on COCOStuff-10K test set.** GFLOPs are measured in resolution 512×512 .

Method	Backbone	GFLOPs	MParams	Pixel Acc (%)	mIoU (%)
PSPNet [18]	MobileNetV2	06.22	02.31	57.4	20.9
DeepLabV3 [29]	MobileNetV2	07.66	02.71	59.2	23.3
DeepLabV3+ [19]	MobileNetV2	07.93	03.21	60.1	23.7
LR-ASPP [30]	MobileNetV3-Small	05.67	01.33	57.5	21.4
LR-ASPP [30]	MobileNetV3	08.83	03.54	58.8	22.7
SegFormer [20]	MiT-B0	07.10	03.88	54.6	27.2
SegFormer [20]	MiT-B1	13.55	13.81	56.6	30.9
SegFormer [20]	MiT-B2	21.71	24.82	58.9	34.3
Segmenter [23]	ViT-Tiny	06.66	06.83	65.0	31.1
Segmenter [23]	ViT-Small	20.01	27.47	69.1	38.2
MaskFormer [31]	Swin-Tiny	07.52	07.63	64.7	31.0
MaskFormer [31]	Swin-Small	20.88	28.55	68.8	38.1
Mask2Former [32]	Swin-Tiny	07.76	07.91	64.5	30.7
Mask2Former [32]	Swin-Small	21.12	29.02	68.5	37.7
MateViT (ours)	ViT-Tiny	04.35	07.98	65.6	31.6
MateViT (ours)	ViT-Small	15.63	29.47	70.2	38.9

Table I summarizes the quantitative comparison with other state-of-the-art methods. Since our aim is to make vanilla ViT [11] more efficient and feasible in real-world applications, for a fair comparison, we mainly compare against plain-ViT-based methods. As shown in Table I, thanks to the learnable importance sampling, our model using ViT-Tiny as the backbone has the smallest GFLOPs (4.35) compared to other CNN- and attention-based methods, while keeping competitive pixel accuracy and mean intersection over union (mIoU). Moreover, regarding the ViT-Small backbone version, our model achieves the best pixel accuracy (70.2%) and mIoU (38.9%) among other counterparts. These results verify the superiority and efficiency of our model with learnable importance sampling for general object segmentation.

C. Results on Material Segmentation

Similar to the experiment on object segmentation, we conduct another experiment on material segmentation using the DMS dataset [13] with the same model architecture and settings. Results are reported in Table II. It can be observed that our model using the ViT-Tiny backbone still has the lowest computation expense (4.30 GFLOPs) with high performance (44.1% in mIoU), and the ViT-Small variant outperforms other methods listed in Table II in both pixel accuracy and mIoU. Furthermore, Fig. 3 presents the per-class IoU of all material categories. It is worth noting that our ViT-Small variant achieves performance gains in all 46 categories, especially the ones that are relevant for assisting PVI, *e.g.*, *fire* (gaining +20.2%), *snow* (gaining +21.3%), *plastic* (gaining +22.6%), and *ceramic* (gaining +25.5%). The aforementioned results prove that our model with learnable importance sampling is capable of achieving high performance and efficiency, not only on the object segmentation but also on the material segmentation task. The high accuracy scores ensure that the effectiveness of our proposed system to assist PVI to recognize materials.

D. Results on Multi-task Learning

To deliver richer dense information to PVI and to perform complementary training, we further conduct experiments on multi-task learning based on our MMoE-based ViT models, taking both object and material segmentation into account.

TABLE II: **Results of single-task learning on DMS dataset.** Values are for the val / test set, respectively. GFLOPs are measured in resolution 512×512 .

Method	Backbone	GFLOPs	MParams	Pixel Acc (%)	mIoU (%)
PSPNet [18]	MobileNetV2	06.12	02.13	66.5 / 66.3	26.1 / 25.9
DeepLabV3 [29]	MobileNetV2	07.52	02.58	68.4 / 68.1	29.8 / 29.7
DeepLabV3+ [19]	MobileNetV2	07.85	03.11	69.3 / 69.2	30.1 / 29.9
LR-ASPP [30]	MobileNetV3-Small	05.41	01.14	66.8 / 66.5	26.5 / 26.4
LR-ASPP [30]	MobileNetV3	08.78	03.29	70.7 / 70.2	30.3 / 29.9
DMS [13]	ResNet-50	-	-	73.1 / 72.9	43.5 / 42.0
SegFormer [20]	MiT-B0	06.95	03.73	60.1 / 59.7	38.5 / 37.4
SegFormer [20]	MiT-B1	13.43	13.69	61.9 / 61.8	41.0 / 41.0
SegFormer [20]	MiT-B2	21.45	24.73	62.4 / 43.2	43.2 / 42.8
Segmenter [23]	ViT-Tiny	06.52	06.76	77.0 / 76.9	44.3 / 43.2
Segmenter [23]	ViT-Small	19.89	27.05	79.5 / 79.0	50.2 / 49.2
MaskFormer [31]	Swin-Tiny	07.22	07.41	76.5 / 76.1	43.8 / 43.2
MaskFormer [31]	Swin-Small	20.36	28.14	78.7 / 78.6	49.7 / 49.1
Mask2Former [32]	Swin-Tiny	07.51	07.77	76.2 / 76.1	43.2 / 43.1
Mask2Former [32]	Swin-Small	20.94	28.55	78.6 / 78.3	49.5 / 49.4
MateViT (ours)	ViT-Tiny	04.30	07.78	76.9 / 76.8	45.3 / 44.1
MateViT (ours)	ViT-Small	15.54	28.79	79.6 / 79.4	51.0 / 50.1

TABLE III: **Results (mIoU) of multi-task learning on COCOStuff-10k and DMS test sets.** GFLOPs are measured in resolution 512×512 .

Method	Backbone	GFLOPs	MParams	COCOStuff (%)	DMS (%)
Trans4Trans [10]	MiT-B0	12.24	04.16	27.7	37.1
Trans4Trans [10]	MiT-B1	18.98	14.26	30.6	41.3
Trans4Trans [10]	MiT-B2	27.00	25.30	34.5	44.1
MateViT (ours)	ViT-Tiny	07.95	11.62	32.7	45.1
MateViT (ours)	ViT-Small	22.08	37.10	40.2	51.1

Table III illustrates the quantitative results. Compared to Trans4Trans MiT-B0 [10], our model using ViT-Tiny as the backbone requires less computation expenses (~35.0% GFLOPs) and comparable number of parameters, while maintaining higher performance on both dataset. Additionally, compared to the Trans4Trans MiT-B2 variant [10], it becomes evident that our ViT-Small variant has a higher mIoU on both COCOStuff-10K (gaining +5.7%) and DMS (gaining +7.0%). In general, the ViT-based models do have a larger number of parameters than the baselines. Compared with the number of parameters (MParams) affecting the size of model, the computational complexity more critically determines the efficiency of the model running on the mobile platform, therefore, affects the fluency of the entire system. According to the single-task results in Table I and Table II, it is worth noting that there are sufficient performance improvements when adding the MMoE layer to our multi-task learning model. The mIoU of ViT-Tiny model is raised from 31.6% (Table I) to 32.7% (Table III) on object segmentation and from 44.1% (Table II) to 45.1% (Table III) on material segmentation. The performance gains are consistent in the ViT-Small variant, from 38.9% to 40.2% and from 50.1% to 51.1% on object- and material segmentation, respectively. The reason for the gains is two-fold: (1) the MMoE layer enlarges the model capacity; (2) when applying MMoE to both object segmentation and material segmentation, the former prevents the latter from overfitting and vice versa.

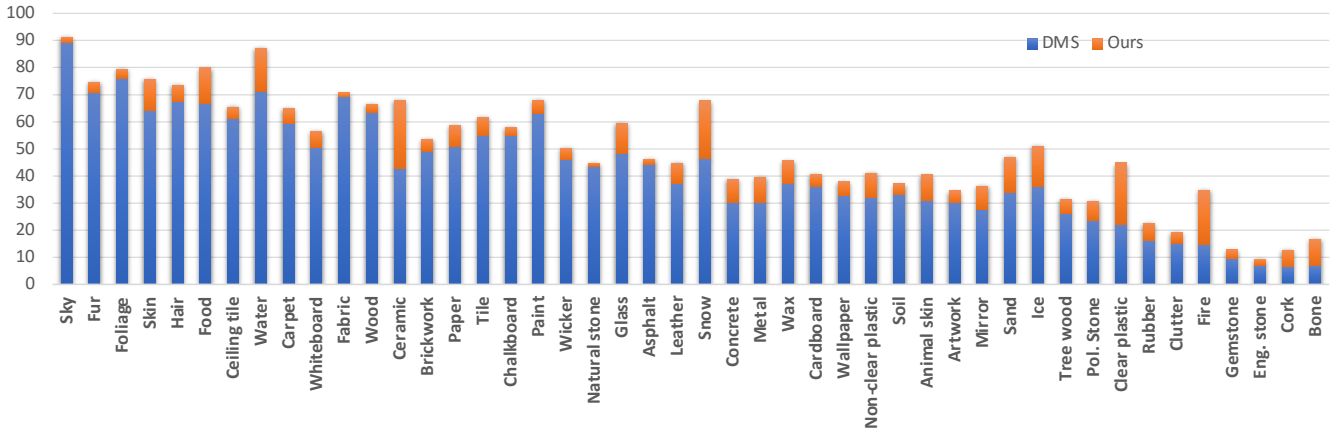


Fig. 3: **Per-class IoU (%) of all material categories.** The blue bar shows the category IoU (%) of the baseline DMS [13], while the orange shows the performance gain (%) of our ViT-Small variant.

E. Ablation Study

To fully understand the proposed methods, an ablation study is conducted regarding the different modules of our model. The quantitative results are shown in Table IV. Our baseline model is the same as Segmenteer ViT-Tiny [23]. Learned from Table IV, replacing ViT-Tiny with ViT-Small as the backbone boosts the performance from 43.2% to 49.2% on mIoU in material segmentation task. After applying LIS, the mIoU continuously increases from 49.2% to 50.1%. We then add the MoE layer to our model, leading to an even higher mIoU of 50.7%. These performance gains also occur on other metrics and in other tasks. It can be observed that our MMoE model achieves the best performances on all metrics in both object segmentation and material segmentation tasks compared to the baseline model, *i.e.*, 6.5% and 3.7% boosts in pixel accuracy, 8.9% and 7.9% boosts in mIoU. Through the extensive pre-study experiments, the effectiveness of the proposed methods can be comprehensively proved.

TABLE IV: **Ablation study** on COCOSTuff-10K and DMS. All values are calculated with testsets.

Method	COCOSTuff-10K		DMS	
	Pixel Acc (%)	mIoU (%)	Pixel Acc (%)	mIoU (%)
Segmenteer [23]	65.0	31.3	76.9	43.2
+ ViT-Small	69.1	38.2	79.0	49.2
+ LIS	70.2	38.9	79.4	50.1
+ MoE	70.8	39.4	79.9	50.7
+ MMoE (MateViT)	71.5	40.2	80.6	51.1

F. Qualitative Analysis

Four groups of scenarios related to the daily life of PVI are shown in Fig. 4, where the original RGB input image, the object segmentation result, and the material segmentation result, are listed in order. The upper-left group describes a scenario where people with visual impairments are having their meals. The *hot dog* colored orange is perfectly recognized by our system in the second image, and it is tagged with a food property according to the material

segmentation result in the third image. The group in the lower left corner shows a scenario where blind people walk in a park. According to the predictions in the second and third images, blind people using our system know additionally there is an asphaltic road ahead. With the additional material information, they can traverse through the road more safely. In the bottom-right case, the entrance is not recognized if only object recognition is performed, however, the material segmentation result can provide supplementary information to find the doors, which can further improve the mobility accessibility. As a result, these dense information can help PVI better understand their surroundings, and to support them to make correct interactions with the environment.

V. USER STUDY

Following detailed pre-study experiments based on datasets, for wearable robotic systems, a critical factor that needs to be addressed is whether the system can provide a positive user experience in real-world situations. To know about that, we conduct a user study in a structured manner, including task-oriented testing and a questionnaire session.

A. Organization

To verify the usability of the system, we further organize a user study with six blindfolded participants on real-world testing scenarios. For the user study, we select seven categories of materials that are common in daily life, *i.e.*, *fabric*, *foliage*, *glass*, *metal*, *paper*, *plastic*, and *wood*. To conduct a comparison between without and with using our system, there are two rounds of material recognition, *i.e.*, **contact** and **contactless** round. The contact round is to recognize by touch, while the contactless round is to recognize by using our system. Note that, to conduct a fair comparison, the order of the two rounds is randomized. Six blindfolded participants (three males and three females) are invited to conduct both testing rounds in the user study, as presented in Fig. 5. In the contact round, the participants are required to name the material after touching an object. The reaction time from touching the object until naming the material is recorded by the organizer. In the contactless round, the participants

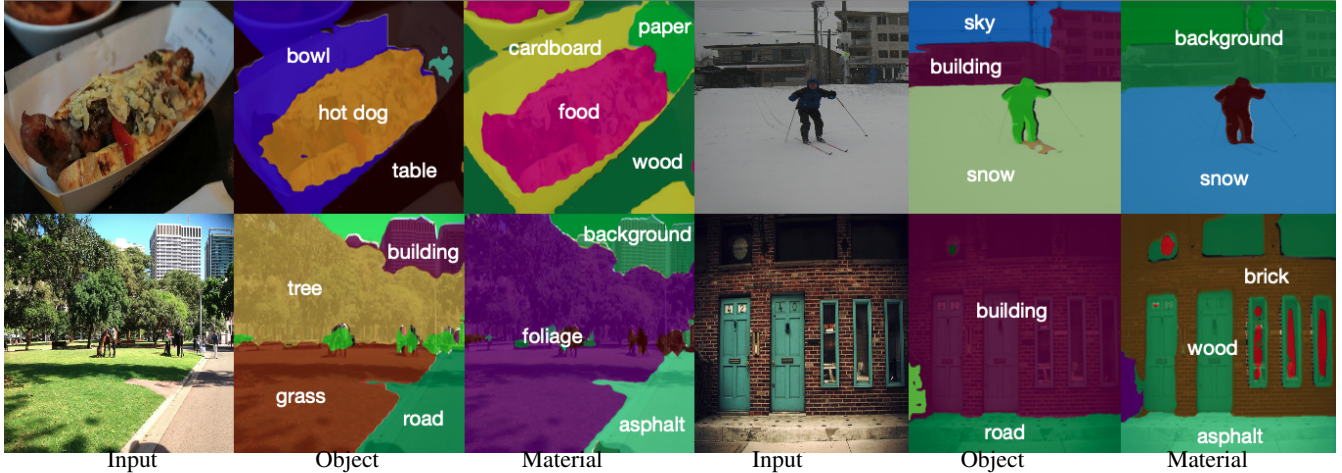


Fig. 4: **Visualization** of both general object segmentation and material segmentation. From left to right in each group: RGB input, object segmentation, and material segmentation.



Fig. 5: Incidences of participants on the user study.

are required to name the material after hearing the feedback from the bone-conduction earphones of the wearable system. The reaction time from starting our system until naming the material is also recorded for the sake of comparison. Apart from the recorded reaction time, answer correctness is another metric of this user study. After two rounds of material recognition, the participants join an anonymous questionnaire session. The questionnaires regarding NASA-Task Load Index (NASA-TLX) and System Usability Scale (SUS) are filled out by all participants. Besides, there is space for participants to write down their open comments.

B. Results

Performance. We utilize average reaction time and answer correctness to evaluate our system performance. Table V presents results on the aforementioned metrics among all participants. While the answer correctness is (100%) in both rounds, the average reaction time in the contactless round is obviously shorter than the contact round (response -0.86 s). Without any haptic perception, our wearable system can perform a faster recognition than the contact-based perception, which indicates our MATERobot is feasible and reliable to provide fast assistance of recognizing material properties via visual cues, and it is able to offer a promising step towards improving the perception accessibility for PVI.

Cognitive load. To learn about the cognitive load of our wearable system, NASA-TLX is a simple and effective method for cognitive load measurement. We first calculate the average score of every factor among all participants. There are six factors, which are *Mental Demand*, *Physical*

TABLE V: Average reaction time and answer correctness in two rounds of material recognition.

	Reaction time (s)	Correctness (%)
Contact round (with touch)	3.97 ± 0.34	100
Contactless round (with our system)	3.11 ± 0.21	100

Demand, Temporal Demand, Performance, Effort, and Frustration. As shown in Fig. 6, we then average the scores of all six factors, resulting in a final NASA-TLX value of 28. According to [33], this value illustrates the workload caused by our system is in the 20th percentile of global workload scores from 6.21 to 88.50 among 1173 observations, which can assist users without too much burden. From Fig. 6, we notice that the effort value is relatively smaller than the rest five factors, meaning that our system is user-friendly.

Usability. Apart from NASA-TLX, we verify the usability of our system with SUS. Our system scores 77 out of 100, which is a relatively high score. According to Bangor *et al.* [34], who analyzed 2324 surveys from 206 studies, “*the best quarter of studies range from 78.51 to 93.93*”. Therefore, we reach that our system is useful for recognizing not only general objects but also their material properties.

User comments. We analyze the open comments made by users during the testing and from the post-study questionnaire session. The insights are reported below:

- Besides the easy operation, 66.7% participants were amazed by the fast response of our material recognition system, which is one of the reasons why they would like to use the system.
- Regarding the material recognition, all participants enjoyed the experience. They found our system useful and helpful in the daily life of visually impaired people.
- However, some participants complained about the voice feedback of the glasses, since it kept informing users of the object material without stopping. We also notice this problem and plan to improve the voice feedback in our future work.

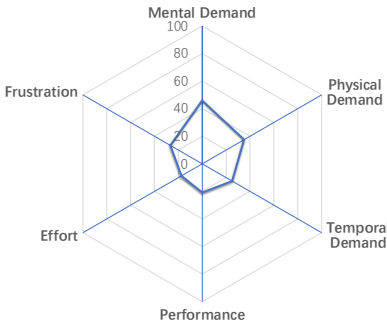


Fig. 6: **Average NASA-TLX score** of every factor among all participants. Values range from 0 to 100, lower is better.

Limitations. Due to the challenges posed by the pandemic, it was difficult to find a sufficient number of participants to perform user study on the developed system. As a result, the system was tested by a limited number of blindfolded participants. While the preliminary field test provides some insights into the potential usefulness of the wearable robotics, the results cannot be considered representative of the experience of real blind users. Another limitation is the lack of diversity among the participants. Without a more diverse range of users, the results may be biased towards certain types of users, which could limit the usefulness in real-world settings. Therefore, in our future work, further research and testing are planned to verify the usability and effectiveness of our wearable robotics with a wide variety of real blind users.

VI. CONCLUSIONS

In this work, we look into semantic material understanding for helping visually impaired people via a wearable robotic system MATERobot. We put forward MATEViT, which unifies general object and material segmentation via a multi-gate mixture-of-experts architecture, whose efficiency is enhanced via token importance sampling to make plain-vision-transformer models suitable for mobile applications. The proposed model is ported to our established assistive MATERobot system designed for supporting people with visual impairments. Extensive experiments on DMS and COCOSTuff-10K datasets and a user study demonstrate the effectiveness and usefulness of our recognition system.

REFERENCES

- [1] D. Yoon and Y. Choi, “Analysis of fingertip force vector for pinch-lifting gripper with robust adaptation to environments,” *T-RO*, 2021.
- [2] L. Ding, L. Huang, S. Li, H. Gao, H. Deng, Y. Li, and G. Liu, “Definition and application of variable resistance coefficient for wheeled mobile robots on deformable terrain,” *T-RO*, 2020.
- [3] K. Yang, L. M. Bergasa, E. Romera, X. Huang, and K. Wang, “Predicting polarization beyond semantics for wearable robotics,” in *Humanoids*, 2018.
- [4] W. Mao, J. Zhang, K. Yang, and R. Stiefelhagen, “Panoptic intention network: Towards efficient navigational perception for the visually impaired,” in *RCAR*, 2021.
- [5] M. Paterson, “‘seeing with the hands’: Blindness, touch and the enlightenment spatial imaginary,” *British Journal of Visual Impairment*, 2006.
- [6] R. Klatzky and S. Lederman, “Object recognition by touch,” in *Blindness and Brain Plasticity in Navigation and Object Perception*, 2007.
- [7] P.-J. Duh, Y.-C. Sung, L.-Y. F. Chiang, Y.-J. Chang, and K.-W. Chen, “V-eye: A vision-based navigation system for the visually impaired,” *TMM*, 2021.
- [8] S. Agrawal, M. E. West, and B. Hayes, “A novel perceptive robotic cane with haptic navigation for enabling vision-independent participation in the social dynamics of seat choice,” in *IROS*, 2022.
- [9] H. Liu, R. Liu, K. Yang, J. Zhang, K. Peng, and R. Stiefelhagen, “HIDA: Towards holistic indoor understanding for the visually impaired via semantic instance segmentation with a wearable solid-state LiDAR sensor,” in *ICCVW*, 2021.
- [10] J. Zhang, K. Yang, A. Constantinescu, K. Peng, K. Müller, and R. Stiefelhagen, “Trans4Trans: Efficient transformer for transparent object and semantic scene segmentation in real-world navigation assistance,” *T-ITS*, 2022.
- [11] A. Dosovitskiy *et al.*, “An image is worth 16x16 words: Transformers for image recognition at scale,” in *ICLR*, 2021.
- [12] H. Caesar, J. Uijlings, and V. Ferrari, “COCO-stuff: Thing and stuff classes in context,” in *CVPR*, 2018.
- [13] P. Upchurch and R. Niu, “A dense material segmentation dataset for indoor and outdoor scene parsing,” in *ECCV*, 2022.
- [14] H. Wang, R. K. Katschmann, S. Teng, B. Araki, L. Giarré, and D. Rus, “Enabling independent navigation for visually impaired people through a wearable vision-based feedback system,” in *ICRA*, 2017.
- [15] A. Aladren, G. López-Nicolás, L. Puig, and J. J. Guerrero, “Navigation assistance for the visually impaired using RGB-D sensor with range expansion,” *IEEE Syst. J.*, 2016.
- [16] J. Long, E. Shelhamer, and T. Darrell, “Fully convolutional networks for semantic segmentation,” in *CVPR*, 2015.
- [17] L.-C. Chen, G. Papandreou, I. Kokkinos, K. Murphy, and A. L. Yuille, “DeepLab: Semantic image segmentation with deep convolutional nets, atrous convolution, and fully connected CRFs,” *TPAMI*, 2018.
- [18] H. Zhao, J. Shi, X. Qi, X. Wang, and J. Jia, “Pyramid scene parsing network,” in *CVPR*, 2017.
- [19] L.-C. Chen, Y. Zhu, G. Papandreou, F. Schroff, and H. Adam, “Encoder-decoder with atrous separable convolution for semantic image segmentation,” in *ECCV*, 2018.
- [20] E. Xie, W. Wang, Z. Yu, A. Anandkumar, J. M. Alvarez, and P. Luo, “SegFormer: Simple and efficient design for semantic segmentation with transformers,” *NeurIPS*, 2021.
- [21] K. He, X. Zhang, S. Ren, and J. Sun, “Deep residual learning for image recognition,” in *CVPR*, 2016.
- [22] A. Vaswani *et al.*, “Attention is all you need,” in *NeurIPS*, 2017.
- [23] R. Strudel, R. Garcia, I. Laptev, and C. Schmid, “Segmenter: Transformer for semantic segmentation,” in *ICCV*, 2021.
- [24] Y. Liang, C. Ge, Z. Tong, Y. Song, J. Wang, and P. Xie, “Not all patches are what you need: Expediting vision transformers via token reorganizations,” in *ICLR*, 2022.
- [25] J. L. Ba, J. R. Kiros, and G. E. Hinton, “Layer normalization,” *arXiv preprint arXiv:1607.06450*, 2016.
- [26] N. Shazeer *et al.*, “Outrageously large neural networks: The sparsely-gated mixture-of-experts layer,” in *ICLR*, 2017.
- [27] I. Loshchilov and F. Hutter, “SGDR: Stochastic gradient descent with warm restarts,” in *ICLR*, 2017.
- [28] M. Contributors, “MMSegmentation: Openmmlab semantic segmentation toolbox and benchmark,” <https://github.com/open-mmlab/mms Segmentation>, 2020.
- [29] L.-C. Chen, G. Papandreou, F. Schroff, and H. Adam, “Rethinking atrous convolution for semantic image segmentation,” *arXiv preprint arXiv:1706.05587*, 2017.
- [30] A. Howard *et al.*, “Searching for MobileNetV3,” in *ICCV*, 2019.
- [31] B. Cheng, A. Schwing, and A. Kirillov, “Per-pixel classification is not all you need for semantic segmentation,” in *NeurIPS*, 2021.
- [32] B. Cheng, I. Misra, A. G. Schwing, A. Kirillov, and R. Girdhar, “Masked-attention mask transformer for universal image segmentation,” in *CVPR*, 2022.
- [33] R. A. Grier, “How high is high? A meta-analysis of nasa-tlx global workload scores,” in *Proceedings of the Human Factors and Ergonomics Society Annual Meeting*, 2015.
- [34] A. Bangor, P. T. Kortum, and J. T. Miller, “An empirical evaluation of the system usability scale,” *Intl. Journal of Human-Computer Interaction*, 2008.